Fang *et al. Energy Mater* 2024;4:400039
DOI: 10.20517/energymater.2023.139

Energy Materials

Article

Open Access

Check for updates

Dendrite-free Zn anodes enabled by interface engineering for non-alkaline Zn-air and Zn-ion batteries

Tao Fang[#], Mengxue Wu[#], Feiyu Lu[#], Zhengyi Zhou, Yanpeng Fu[*], Zhicong Shi[*]

Institute of Batteries, School of Materials and Energy, Guangdong University of Technology, Guangzhou 510006, Guangdong, China.
[#]Authors contributed equally and co-first authors.

***Correspondence to:** Yanpeng Fu, School of Materials and Energy, Guangdong University of Technology, No. 100 Waihuan Xi Lu, Guangzhou Higher Education Mega Center, Panyu District, Guangzhou 510006, Guangdong, China. E-mail: fuyanpeng@gdut.edu.cn; Prof. Zhicong Shi, School of Materials and Energy, Guangdong University of Technology, No. 100 Waihuan Xi Lu, Guangzhou Higher Education Mega Center, Panyu District, Guangzhou 510006, Guangdong, China. E-mail: zhicong@gdut.edu.cn

How to cite this article: Fang T, Wu M, Lu F, Zhou Z, Fu Y, Shi Z. Dendrite-free Zn anodes enabled by interface engineering for non-alkaline Zn-air and Zn-ion batteries. *Energy Mater* 2024;4:400039. https://dx.doi.org/10.20517/energymater.2023.139

Received: 30 Dec 2023 **First Decision:** 5 Mar 2024 **Revised:** 1 Apr 2024 **Accepted:** 15 Apr 2024 **Published:** 6 May 2024

Academic Editors: Bin Wang, Ahmad Amiri **Copy Editor:** Fangling Lan **Production Editor:** Fangling Lan

Abstract

Aqueous zinc-metal batteries hold immense promise for large-scale energy storage applications due to their cost-effectiveness and superior safety features. However, uncontrolled dendrite growth, corrosion and side reactions in aqueous environments destabilize the electrode/electrolyte, leading to Zn plating/striping irreversibility. Herein, a low-cost, non-toxic functional electrolyte additive, tetraethyl ammonium bromide (TEAB), addresses this challenge. The preferential adsorption of TEAB on the surface of the Zn anode endows the Zn/electrolyte interface with an optimized electric field distribution and abundant active sites for the uniform and dendrite-free Zn^{2+} deposition. Moreover, TEAB disrupts the H-bond network between the electrolytes, effectively suppressing water-induced side reactions and corrosion. Consequently, a Zn||Zn symmetric battery achieves a long cycle life of 4,950 h at 1 mA cm^{-2}, and the average coulombic efficiency of the Zn||Cu battery reaches as high as 99.5%. Additionally, even after 2,000 cycles at 3 A g^{-1}, the capacity retention of the Zn||MnO_2 battery remains at 91.22%. The non-alkaline full Zn||air batteries deliver remarkable cycling stability up to 270 h.

Keywords: Additives, dendrite free, tetraethyl ammonium bromide, Zn anodes

INTRODUCTION

In recent years, the design of cost-effective, environmentally friendly, and reusable secondary batteries has emerged as an ideal solution for electrochemical energy storage devices (EESDs) across various industries[1-3]. Ever since their commercialization, lithium-ion batteries (LIBs) have become the preeminent energy storage technology in electric vehicles, portable electronic devices, and various other energy advancement domains[4,5]. However, obstacles to their construction automation primarily stem from challenges, including the scarcity of lithium resources, safety concerns linked to flammable organic electrolytes, and the significant costs involved[6-9]. Consequently, alternative metal-based EESDs, including Zn, Na, Ca, Al and K, have gained increasing attention. Among these options, zinc-based EESDs, such as zinc-ion batteries (ZIBs) and zinc-air batteries (ZABs), hold significant potential in energy storage[10]. Zinc, serving as a plentiful and easily obtainable anode material, offers a high theoretical volume capacity density (5,585 mAh cm^{-2}), low redox potential [E (Zn/Zn^{2+}) = 0.76 V *vs.* the standard hydrogen electrode (SHE)], environmental friendliness, low-cost, and wide applicability[5,11,12]. Furthermore, due to its inherently safe aqueous inorganic electrolyte composition, zinc-based EESDs display simplified battery manufacturing processes with reduced environmental pollution and costs and high ionic conductivity (> 10 mS cm^{-1})[13].

Nevertheless, the uncontrolled growth and parasitic reaction of zinc dendrites pose a significant challenge for zinc anodes in zinc-metal batteries (ZMBs), severely limiting their practical application[14-16]. Among various strategies explored so far, optimizing aqueous electrolytes by incorporating additives has emerged as one of the most cost-effective and feasible solutions to address these issues[17,18]. The primary objective behind this strategy is to enhance the electrochemical environment. Meanwhile, beneficial elements are deposited or adsorbed on the Zn electrode, which promotes uniform electric field, improves the deposition morphology of Zn^{2+}, inhibits corrosion, and prevents passivation[19-21]. However, identifying an additive that can simultaneously cater to the requirements of both aqueous ZIBs (AZIBs) and ZABs remains a formidable task.

Highly concentrated alkaline electrolytes (6-7 M KOH) were widely studied for ZABs, while few researches focused on weak acidic and neutral electrolytes[22-24]. Zn anodes in alkaline electrolytes are prone to the dendrite formation, alkali-inert by-product generation, and continuous corrosion during charge and discharge, leading to obvious passivation on the anode surface[25,26]. Excessively using anodes and electrolytes to improve battery performance is not only material waste but also underutilizes battery capacity. Moreover, overabundant alkaline electrolytes tend to degrade during operation and readily react with CO_2 in the atmosphere, reducing electrical conductivity[27]. Employing a pure O_2 environment as a solution to cathode introduces additional costs and complicates the system, thereby diminishing its commercial viability. To address this issue, most AZIBs apply neutral or slightly acidic baseline electrolytes such as zinc sulfate ($ZnSO_4$), zinc chloride ($ZnCl_2$), Trifluoromethanesulfonic acid zinc salt [$Zn(TfO)_2$], and zinc acetate [$Zn(CH_3CO_2)_2$][24,25]. By combining these baseline electrolytes with various low concentration additives, distinct inhibitory effects on the dendrite formation and side reactions can be achieved, significantly enhancing cycle stability. Inspired by this, incorporating neutral or slightly acidic electrolytes into ZABs presents a promising avenue[2,19]. Non-alkaline electrolytes offer many advantages and hold great research significance. Firstly, they generally exhibit high reversibility for the Zn deposition. Secondly, the electrolyte remains unreactive towards CO_2, ensuring battery stability in the air environment. However, exposing the electrode to the aqueous solution environment still results in numerous side reactions, necessitating the introduction of appropriate additives to enhance the electrolyte properties[28,29].

Quaternary ammonium organic surfactant additives significantly inhibit dendrite and by-product formation and corrosion in AZIBs and alkaline ZABs. Trace amounts of tetrabutylammonium sulfate (TBA_2SO_4)[20],

tetraethylammonium chloride (TEAC)[19], and cetyltrimethylammonium bromide (CTAB)[30] introduced into AZIBs as multifunctional additives can reduce the activity of H_2O, adsorb onto the Zn anode surface to optimize Zn deposition direction, and inhibit by-products. Adding methyl ammonium bromide and tetrabutylammonium bromide (TBAB) to alkaline ZAB electrolytes can effectively suppress the formation of ZnO and dendrite growth[31]. The method of introducing additives into non-alkaline electrolytes is rarely observed. Herein, we have developed a non-toxic, low-cost, non-alkaline electrolyte additive strategy for AZIBs and ZABs. By introducing tetraethyl ammonium bromide (TEAB), the H bond network in the electrolyte can be disrupted; interfacial wettability of Zn anodes is improved, and solvation sheath structure of Zn^{2+} is altered. TEAB effectively suppresses dendrite growth and improves the battery reversibility. The Zn||Zn battery exhibits an exceptional cyclic stability of 4,950 h at 1 mA cm^{-2}-1 mAh cm^{-2}. The Zn||MnO_2 battery demonstrates an impressive lifespan exceeding 2,000 cycles at 3 A g^{-1}. Furthermore, the Zn||air battery achieves a reversible capacity of 616 mAh g_{Zn}^{-1} and can undergo cycling for up to 270 h.

EXPERIMENTAL

Preparation of electrolyte

To establish a baseline electrolyte, zinc sulfate ($ZnSO_4 \cdot 7H_2O$, Aladdin, purity of 99%) was dissolved in deionized water (DI water) to obtain a 1 M $ZnSO_4$ solution. Subsequently, TEAB (Aladdin, purity of 99%) was added at varying concentrations to form TEAB-containing electrolytes. All ingredients were placed in sealed bottles and sonicated for 2 h to become uniform and clear.

Cathode preparation

The synthesis of δ-MnO_2 was accomplished using a straightforward redox reaction. Initially, 1.48 g KCl and 0.632 g $KMnO_4$ were combined with 100 mL of DI water. This mixture was stirred for 10 min. Subsequently, the mixed solution was transferred to a water bath maintained at 60 °C. Additionally, 1.014 g $MnSO_4$ was introduced and allowed to react at 60 °C for 60 min. The reaction products were filtered three times in DI water and subsequently dried for 12 h at 70 °C in a vacuum oven. For the fabrication of the δ-MnO_2 cathode, δ-MnO_2, polyvinylidene fluoride (PVDF), and Ketjen black were mixed in a ratio of 7:1:2, using N-methyl-2-pyrrolidone (NMP) as the solvent. The prepared slurry was spread onto carbon cloth, intended for use as cathode materials in AZIBs. This cathode material was then dried in an oven for 12 h. The loading distribution was about 1.5 mg cm^{-2}.

Electrochemical measurements

Zn||Zn, Zn||Cu, Zn||Mo, and Zn||MnO_2 were assembled under ambient conditions. The dimensions of all metal electrodes are 10 mm × 10 mm. The Zn foil has a thickness of 200 μm, and the Cu and Mo foils are each 100 μm thick. Glass fiber (GF/A) served as the separator for all cells. The baseline electrolytes employed were 1 M $ZnSO_4$ for the symmetric and half cells, 1 M $ZnSO_4$ supplemented with 0.1 M $MnSO_4$ for the full cells, and the electrolyte volume was 80 μL. The Zn||air cell used the MnO_2/C air electrode as the cathode and the Zn foil (30 mm × 20 mm) as the anode, which was assembled and tested under ambient air conditions at room temperature. The battery was charged and discharged with a LAND battery tester. Additionally, a CHI660E electrochemical station was employed to test electrochemical impedance spectroscopy (EIS), linear sweep voltammetry (LSV), polarization (Tafel), Chronoamperometry (CA), and cyclic voltammetry (CV).

SS||SS symmetric batteries were assembled and tested through the impedance method to explore the conductivity of electrolytes. The ionic conductivity is determined by:

$$\sigma = L/(RS)$$

where σ denotes the ionic conductivity, L represents the thickness of the electrolyte layer, R signifies the resistance, and A corresponds to the contact area of the electrode.

Material characterizations

Crystallographic data of the samples were acquired at a scanning rate of 10° min^{-1} using a Bruker D8 Advance X-Ray Diffractometer. To investigate the surface structure of the samples, a Hitachi SU-8010 scanning electron microscope (SEM) was used. Prior to SEM measurements, the samples were coated with gold under a nitrogen (N_2) atmosphere. Surface compositions were evaluated using ESCALAB Mk X-ray photoelectron spectroscopy (XPS). Additionally, the Fourier transform infrared (FT-IR) spectrum was obtained using the Spectrum 100. The Raman spectrum was obtained using the Jobin Yvon HORIBA instrument with a laser wavelength of 633 nanometers. The SL250 Contact Angle Measuring System was leveraged to evaluate the contact angles.

RESULTS AND DISCUSSIONS

We consistently adhere to the principle of conducting low-cost and environmentally friendly research in experiments. We select 1 M $ZnSO_4$ as the baseline electrolyte, designated as ZSO, and subsequently incorporated TEAB as an electrolyte additive at concentrations of 0.01, 0.05, and 0.1 M, denoted as × M TEAB. As depicted in Supplementary Figure 1, both ZSO and TEAB at different concentrations remained homogenous, even after standing for 15 days. Furthermore, ignition tests reveal that even with a maximum additive concentration of 0.2 M TEAB [Supplementary Figure 2], high non-flammability levels are maintained.

To demonstrate the capability of TEAB in reducing H_2O molecule activity and inhibiting side reactions, FT-IR spectroscopy, Raman spectroscopy, and nuclear magnetic resonance (NMR) identified various functional groups present in the electrolyte. Figure 1A and B illustrates the detection of the tensile vibration of O-H within the range of 3,000-3,700 cm^{-1}. The blue shift of ν(O-H) peak with the increasing TEAB concentrations (0, 0.01, 0.05, 0.1, 0.2 M) indicates the enhanced bonding ability of O-H groups. This increase in O-H bond energy facilitates disruption of H-bond network between H_2O molecules and significantly suppresses side reactions. The enhanced interaction between TEAB and H_2O molecules reduces the activity of H_2O molecules. Besides, the peaks at 2,956 and 3,002 cm^{-1} observed in the Raman spectrum of TEAB electrolyte are ascribed to the vibrational modes of C-H bonds, exhibiting enhanced intensities with increasing additive concentration[30,32]. As seen in Figure 1C, pure ZSO electrolyte displays a characteristic peak at 982 cm^{-1}, which corresponds to ν(SO_4^{2-}) mainly arising from formation of the contact ion pair (Zn^{2+}-OSO_3^{2-}). In the mixed solution containing both TEAB and ZSO, additional solvent-specific peaks at 667, 897, 1,069 and 1,120 cm^{-1} are detected, suggesting alterations in the coordination between solvents and the chemical environment of the electrolyte[33]. The disruption of solvation structure and the H-bonds network are supported by the ^1H NMR spectra [Figure 1D]. A shift to downfield is observed upon adding ZSO and TEAB, indicating the decreased electron cloud density of H_2O on ^1H and, therefore, the reduced H-bonds interactions between H_2O molecules. The addition of TEAB disrupts the H-bonds network between H_2O and simultaneously optimizes the electrolyte environment to inhibit side reactions.

The wetting behavior of the electrode/electrolyte interface was assessed through a contact angle test [Figure 1E-I]. After resting for 30 s, the Zn electrode with pure ZSO electrolytes exhibits a contact angle of 85.20°. This large contact angle indicates that the Zn electrode surface possesses strong hydrophobicity in

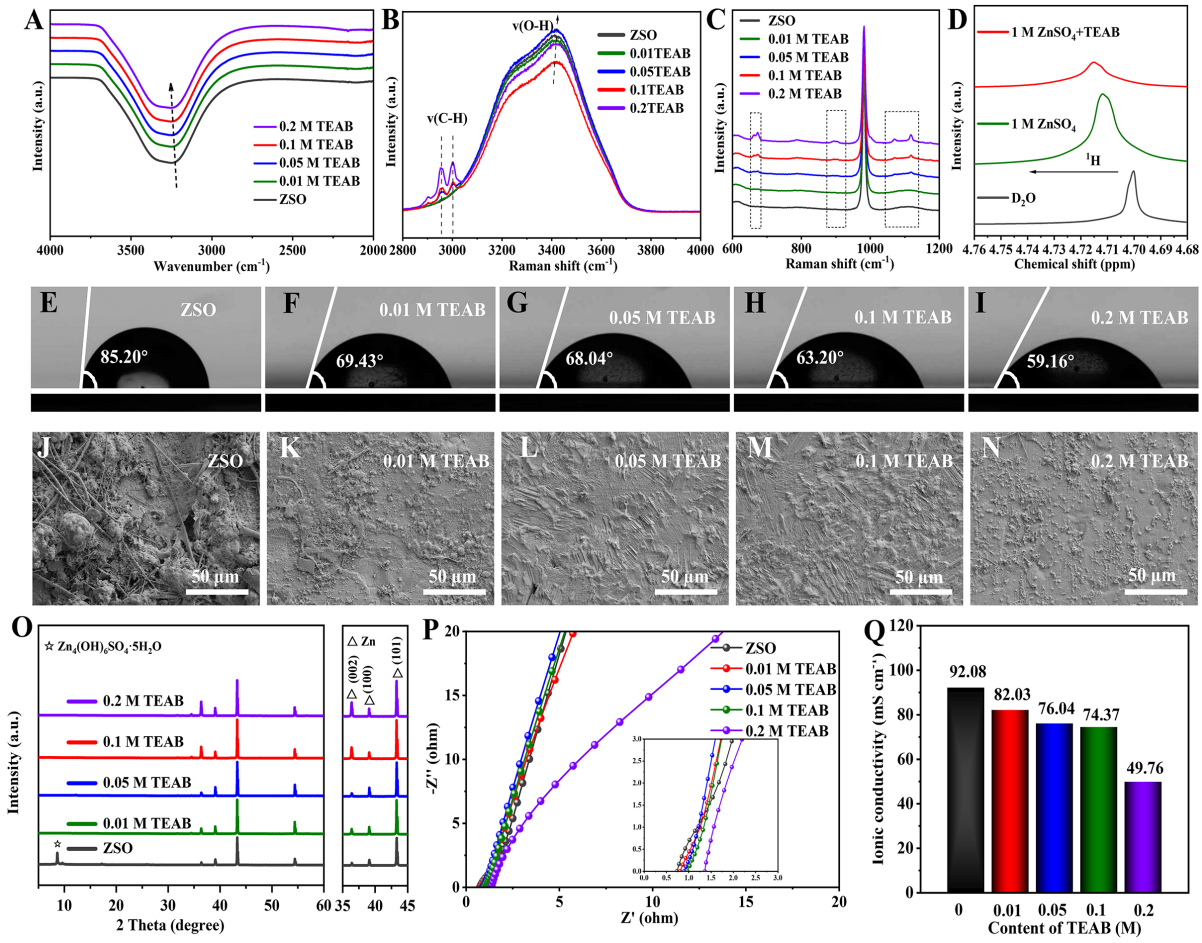

Figure 1. (A) FT-IR and (B and C) Raman spectra in ZSO electrolytes with and without different concentrations of TEAB additives. (D) ^{1}H NMR in ZSO electrolytes with and without TEAB additive. (E-I) Contact angle measurements on Zn electrodes in ZSO electrolytes with and without different concentrations of TEAB additives. (J-N) SEM images of Zn anodes after cycling 100 h in ZSO electrolytes with and without different concentrations of TEAB additives. (O) XRD patterns of Zn anodes cycled after 100 h in ZSO electrolytes with and without different concentrations of TEAB additives. (P) Nyquist plots and (Q) Ionic conductivity images in ZSO electrolytes with and without different concentrations of TEAB additives.

the ZSO electrolyte, thereby impeding continuous wetting of the electrolyte on the Zn electrode. Conversely, incorporating TEAB additives enhances the inherent electrode/electrolyte wettability with the contact angles of 69.43°, 68.04°, 63.20°, and 59.16° for 0.01, 0.05, 0.1, and 0.2 M TEAB, respectively, much lower than that for the ZSO electrolyte. The TEAB additive readily adsorbs onto the Zn electrode surface and exhibits excellent affinity towards Zn^{2+}. Notably, the improved wetting capacity facilitates reversible plating/stripping of Zn^{2+}.

After plating/stripping in the pure ZSO electrolyte, the electrode surface, as observed in Figure 1J, is rather rough with many coarse Zn dendrites and by-products. Regrettably, even Zn particles with tens of microns are sufficient to puncture the separator. In sharp contrast, introducing TEAB additives enhances the electrode surface flatness and inhibits side reactions [Figure 1K-N]. It is noteworthy that Zn electrodes deposited in 0.01 and 0.2 M TEAB electrolytes still exhibit numerous loose fine Zn particles and a few by-products, whereas smooth and compact deposits are observed in 0.05 and 0.1 M TEAB electrolytes. Insufficient or excessive TEAB additives result in uneven deposition layers and ineffective inhibition of dendrite formation and by-product generation. The X-ray diffraction (XRD) results are presented in

Figure 1O. In addition to Zn diffraction peaks, other crystalline phases corresponding to $Zn_4(OH)_6SO_4·5H_2O$ by-products are detected in the pure ZSO electrolyte. Conversely, no by-product is observed with different concentrations of TEAB additives. It is noteworthy that the Zn (002)/Zn (100) ratio (> 1) with TEAB additive surpasses that of pure ZSO (< 1) as the additive concentration increases to 0.1 M. TEAB optimizes the deposited crystal face of Zn^{2+}, dictate the preferred direction of Zn^{2+} deposition, and achieve a compact stacking morphology of Zn.

Ionic conductivity is an important index of the ion transport ability in the electrolyte, which can be determined from the impedance value of a stainless-steel symmetric cell (SS||SS) containing various electrolytes [Figure 1P]. Compared to pure ZSO electrolyte (92.08 mS cm^{-1}), slight decreases in the ionic conductivity are observed with values of 82.03, 76.04, and 74.37 mS cm^{-1}, respectively, with 0.01, 0.05, and 0.1 M TEAB additives [Figure 1Q]. However, the conductivity drops to 49.76 mS cm^{-1} with 0.2 M TEAB. The CV and EIS curves are examined to further elucidate the impact of TEAB additives on conductivity [Supplementary Figures 3 and 4]. With TEAB, a reduction in the peak current in the CV curve can be observed, indicating a decrease in the cell plating kinetics and an increase in the ion transport resistance. The above discussions suggest 0.1 M TEAB additive as the optimal concentration.

Zn||Zn cells were subjected to electrochemical performance tests at various current densities and fixed area capacities to investigate the cycling stability of Zn anodes with and without TEAB additives. As depicted in Figure 2A, at 1 mA cm^{-2}-1 mAh cm^{-2}, the overpotentials of different Zn||Zn cells remain below 100 mV. Pure ZSO electrolytes only provide a cycle life of 87 h after which short circuits occur due to excessive dendrite growth and frequent side reactions. Remarkably, it is worth noting that the Zn||Zn symmetric cell exhibits stable cycling up to 4,950 h in the presence of 0.1 M TEAB electrolyte, approximately 57 times longer than that with pure ZSO electrolytes. TEAB preferentially adsorbs onto the anode surface to provide more active sites for the Zn^{2+} deposition, promoting the formation of tiny Zn nuclei and, therefore, decreasing the dendrite and by-product formation. At a high current density of 5 mA cm^{-2}, the symmetric cell with TEAB additives exhibits a long cycle life of 2,950 h [Figure 2B]. According to the nucleation and growth theory, increasing current density allows for the formation of small and dense Zn nuclei[20]. Even under harsh conditions with increased capacities of 5 mA cm^{-2}, 5 mAh cm^{-2} and 10 mA cm^{-2}, 10 mAh cm^{-2}, symmetric cells in the presence of TEAB additives demonstrate rather stable cycle reversibility, reaching up to 750 and 500 h, respectively [Supplementary Figure 5 and Figure 2C]. The high-rate performance results are presented in Figure 2D and Supplementary Figure 6. Zn||Zn cells in 0.1 M TEAB exhibit excellent cyclic stability within the current density ranging from 1 to 30 mA cm^{-2} under a constant area capacity of 1 mAh cm^{-2}. In contrast, Zn||Zn cells without TEAB show significant voltage fluctuations at current densities above 15 mA cm^{-2}, leading to subsequent cycle short circuits. Similarly, Supplementary Figure 7 shows the rate performance (0.1-5 mA cm^{-2}) at a low current density.

Under reversible Zn cycles of 5 mA cm^{-2} and 0.5 mAh cm^{-2}, the coulombic efficiency (CE) was determined by asymmetric Zn||Cu cells. The cell fails after fewer than 350 cycles in pure ZSO electrolytes. However, with TEAB additives, the average CE of the Zn||Cu cell reaches an impressive 99.5% even after 1,000 cycles [Figure 2E]. This could be well explained that the presence of TEAB can promote homogeneous Zn^{2+} deposition while effectively inhibiting dendrite growth and parasitic reactions. Furthermore, including TEAB additives results in an initial overpotential of 284.5 mV compared to 169.6 mV observed in the pure ZSO electrolyte [Figure 2F], which is consistent with the ionic conductivity analysis. The nucleation and growth of Zn on the Cu surface is hindered, which facilitates the finely crystalline nuclei formation. These nuclei are uniformly distributed across the anode surface, substantially reducing the likelihood of Zn dendrite formation and contributing to generating homogeneous Zn deposits. Consequently, both Zn||Zn

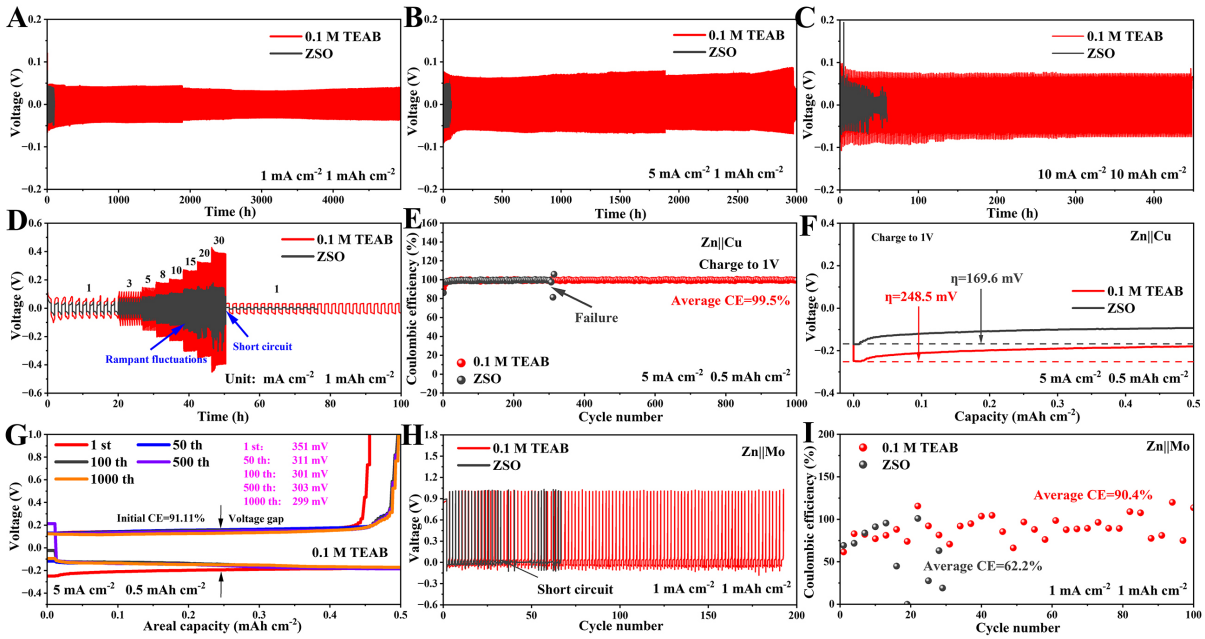

Figure 2. Cycling performance of Zn||Zn cells in ZSO electrolytes with and without 0.1 M TEAB additive under (A) 1 mA cm^{-2} and 1 mAh cm^{-2}, (B) 5 mA cm^{-2} and 1 mAh cm^{-2}, (C) 10 mA cm^{-2} and 10 mAh cm^{-2}. (D) Rate performance at different current densities from 1 to 30 mA cm^{-2} in ZSO electrolytes with and without 0.1 M TEAB additive. (E) CEs of Zn plating/stripping behavior in the Zn||Cu cells. (F) Zn deposition voltage profiles of Zn||Cu asymmetric cells in ZSO electrolytes with and without 0.1 M TEAB additive. (G) corresponding voltage profiles at various cycles with TEAB. (H) Cycling performance and (I) CEs of Zn||Mo cells in ZSO electrolytes with and without 0.1 M TEAB additive.

symmetric cells and Zn||Cu half cells exhibit significantly enhanced cycle life. Figure 2G and Supplementary Figure 8 compare plating/stripping curves of Zn||Cu cells in different electrolytes. In the presence of TEAB additives, the cell exhibits an initial CE value of 91.11%, surpassing that in the absence of TEAB (86.11%). Additionally, the cell with the TEAB additive demonstrates a high and stable voltage gap upon cycling. The cyclic stability of the assembled Zn||Mo cell under the reversible cycling condition of 1 mA cm^{-2} and 1 mAh cm^{-2} is illustrated in Figure 2H. The incorporation of TEAB into the electrolyte results in an extended cycle life and enhances the cycle stability of the cell. Simultaneously, a higher average CE (90.4%) of the Zn||Mo cell with TEAB additives can be obtained compared to 62.2% in the pure ZSO electrolyte [Figure 2I]. The aforementioned results illustrate that adding a small amount of TEAB additive can facilitate Zn electrodes in achieving commendable CE, enhanced capacity retention, and prolonged cycling stability.

The SEM image in Figure 3A and B illustrates the nickel foam galvanized at the constant voltage of 0.1 V. Loose lamellar stacking morphology and petal-like Zn dendrites could be obviously observed in the pure electrolytes, as compared to a compact hexagonal crystal in the presence of TEAB additives. LSV curves of different electrolytes at 10 mV cm^{-2} are shown in Figure 3C, which can be used to evaluate the electrochemical window and hydrogen evolution reaction (HER) of the electrolyte. The electrochemical stability window (ESW) increases by 55 mV with the addition of TEAB additives. In addition, the enhanced HER overpotential while reduced HER current density indicates the successful hinderance of H_2O-induced HER with the TEAB additive. Simultaneously, we conducted corrosion stability tests on the electrode surface with various additives. The Tafel polarization curve in Figure 3D reveals that incorporating TEAB elevates the corrosion potential on the Zn electrode surface from -0.997 to -0.985 V. Consequently, the TEAB addition effectively mitigates the corrosion tendency of the Zn electrode and exhibits remarkable

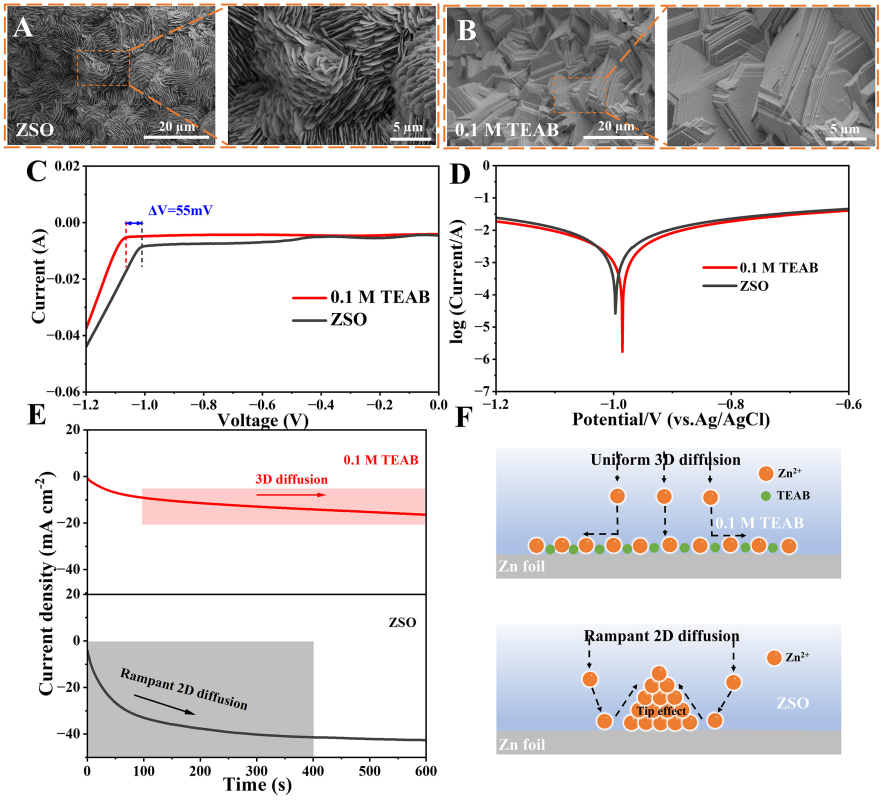

Figure 3. (A and B) SEM images of the Ni foam galvanized in ZSO electrolytes with and without 0.1 M TEAB additive at the constant voltage of -0.1 V (*vs.* Zn/Zn^{2+}) for 0.5 h. (C) LSV of different electrolytes at 10 mA cm^{-2}. (D) Tafel curves at 1 mV s^{-1}. (E) CA curves of different electrolytes at an overpotential of -150 mV. (F) Deposition models of Zn^{2+} in ZSO electrolytes with and without 0.1 M TEAB additive.

anti-corrosion capabilities. The SEM images in Supplementary Figure 9 illustrate the surface morphology of the Zn foils immersed in various electrolytes for a week. Notably, severe corrosion can be observed when exposed to pure ZSO electrolytes, accompanied by the formation of granular basic zinc sulfate by-products. Conversely, no corrosion or by-product formation occurs when using TEAB additives. In addition, CA was conducted at -150 mV to assess the diffusion and deposition mechanism of Zn^{2+} in different electrolytes [Figure 3E]. The Zn electrode immersed in the pure ZSO electrolyte exhibits a continuously decreasing current density, suggesting a continuous two-dimensional (2D) diffusion. During 2D diffusion, Zn^{2+} undergoes continuous lateral diffusion along the electrode surface, resulting in rampant dendrite growth under the influence of "tip effect", which leads to significant disruption of electric field distribution. Adding a small amount of TEAB can significantly mitigate this phenomenon. The preferential adsorption of TEAB creates a transverse energy barrier for the diffusion of Zn^{2+}, and after a brief period (100 s) of 2D diffusion, stable 3D diffusion is observed for the Zn electrode. A higher energy barrier implies stronger driving force that facilitates spreading out to more active sites for deposition by Zn^{2+}, thereby promoting flat deposition layer formation [Figure 3F][34,35]. The EIS plots at different temperatures and Corresponding activation energy values (E_a) are presented in Supplementary Figure 10. The de-solvation process of Zn^{2+} is investigated by employing the Arrhenius equation (inset of Supplementary Figure 10C) to calculate E_a. It is noteworthy that the E_a value for 0.1 M TEAB (16.7 KJ mol^{-1}) is lower than that of ZSO (24.9 KJ mol^{-1}), confirming that the addition of TEAB could effectively enhance the de-solvation process of Zn^{2+}[36].

With a view to further elucidate the working mechanism of the TEAB additive, the surface composition of the Zn electrode was analyzed by XPS. Exceptionally strong C signals are observed on the Zn electrode surface with TEAB additives [Figure 4A and B], including C-C, C-H, C-N, C-O, and O-C=O, which arise from the organic cations of TEAB additives. Figure 4C and D clearly demonstrates that the intensity of Zn 2p peaks on the ZSO electrode surface is significantly higher than that observed in the TEAB electrolyte, providing further evidence for the presence of a TEAB adsorption layer on the surface. Furthermore, S 2p spectra show a pair of spin-orbit coupling peaks of sulfate situated at 168.75 and 169.9 eV, corresponding to S $2p_{1/2}$ and S $2p_{3/2}$. A notable reduction in the S 2p strength with the TEAB additives suggests the successful inhibition of zinc sulfate hydroxide hydrate (ZSH) by-product formation on the Zn electrode surface [Figure 4E and F].

We further assemble Zn||MnO_2 full cells to demonstrate the practical application potential of the TEAB additive. Supplementary Figure 11 shows the SEM image patterns of the cathode materials δ-MnO_2 obtained via a facile redox method. By comparing the CV curves of both electrolytes, the inclusion of TEAB additives does not induce any additional reactions [Figure 5A][37]. The EIS tests of Zn||MnO_2 full cells in ZSO and 0.1 M TEAB electrolytes are illustrated in Supplementary Figure 12. Using 0.1 M TEAB electrolyte results in an elevated initial impedance for the cell, which aligns consistently with the conductivity results. Additionally, the rate performance demonstrates that the Zn||MnO_2 cell using 0.1 M TEAB electrolyte exhibits superior stability compared to the one with ZSO electrolyte [Supplementary Figure 13]. As seen in Figure 5B, a Zn||MnO_2 cell with the pure ZSO electrolyte exhibits a rapid capacity decay under 1 A g^{-1} with a capacity retention rate of only 33.32% after 500 cycles. Nevertheless, the full cell with TEAB additives demonstrates superior cycle stability. At a higher current density of 3 A g^{-1}, the specific capacity of the cell with pure ZSO electrolyte is only 64.1 mAh g^{-1} (36.15%) after 500 cycles. Furthermore, the cell exhibits a further deterioration with a capacity retention rate of only 30.12% after 2,000 cycles. Conversely, the full cell in the presence of TEAB additives achieves impressive cycling performance, retaining an impressive 91.22% capacity after cycling for 2,000 cycles [Figure 5C].

The effect of the TEAB additives is further evaluated in Zn||air cells, applying air as a cathode in ZSO electrolytes with and without the TEAB additive. The setup is schematically shown in Supplementary Figure 14. As observed in the CV curves in Figure 5D, the onset potentials of oxygen reduction (ORR) and oxygen evolution reactions (OER) in the air cathode side in the pure ZSO electrolyte are about 1.54 and 1.73 V (*vs.* Zn/Zn^{2+}). Adding TAEB to the electrolyte does not result in a prominent ORR peak, but the onset potential of the OER is improved to 1.93 V. This is comparable to the previous study[38], in which the discharge and charge voltages in the neutral electrolyte are around 1.9 and 2.0 V.

Figure 5E compares the cycling performance of ZABs at 0.5 mA cm^{-2} (discharge and charge for 1 h) with different electrolytes. The open-circuit voltages of the cells in both ZSO electrolytes with and without TEAB additives are 1.54 V, close to the one in the alkaline solution. The voltage drops to 0 during discharge in the pure ZSO electrolyte. On the other hand, the ZABs in the presence of TEAB additives can cycle stably for more than 270 h. Adding TEAB additives can improve the dissolution, migration and deposition of Zn^{2+} in the electrolyte, alleviate the contact between the Zn anode and the electrolyte, and form a surface intermediate to alleviate the anodic corrosion. The comparison of the charging and discharging voltages during cycling in the presence of TEAB additives can be seen in Supplementary Figure 15. The gap voltage is 0.86 V, and energy efficiency reaches 53% at the initial 30 h. The gap voltage is 1.09 V, and energy efficiency only reaches 42% after 100 h. Due to the evaporation of the electrolyte in the air, the actual effective contact area between the active material and the electrolyte is reduced, leading to a higher overpotential later. In addition, ZABs with TEAB additives can achieve a reversible capacity of 616 mAh g^{-1}

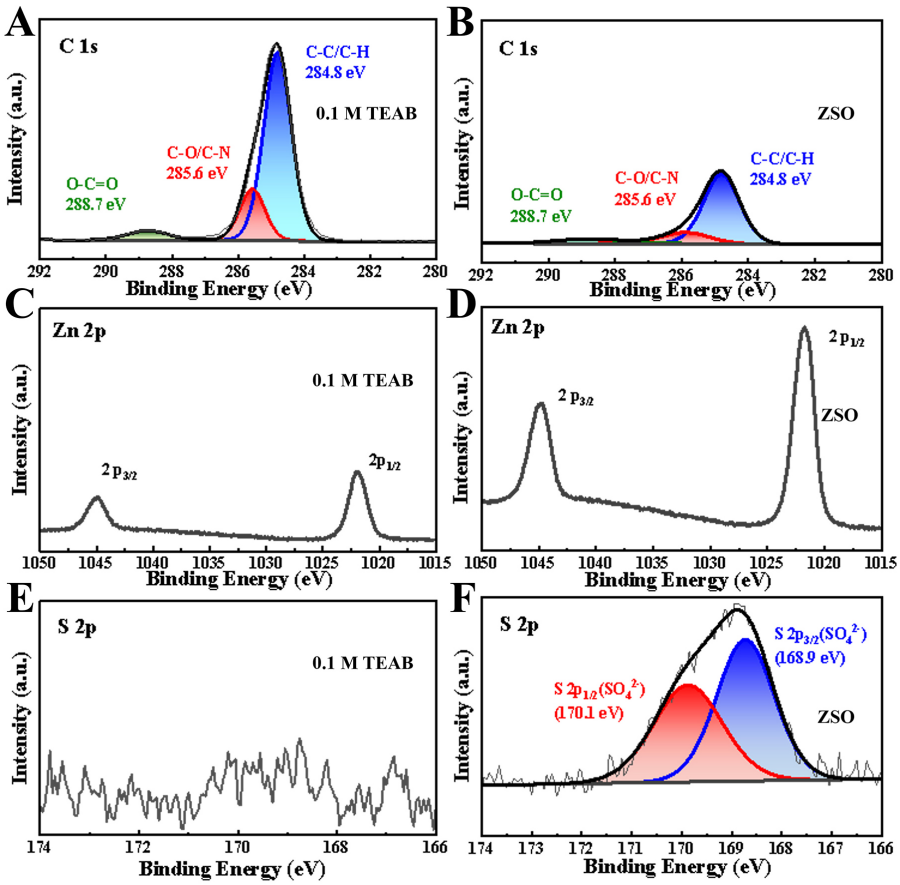

Figure 4. XPS spectra of Zn anodes after 15 cycles in ZSO electrolytes with and without 0.1 M TEAB additive: High-resolution XPS spectra of (A and B) C 1s, (C and D) Zn 2p and (E and F) S 2p.

[Supplementary Figure 16]. SEM images show that the cycled Zn anode in the pure ZSO electrolyte exhibits a rough surface with many deep pits [Figure 5F]. On the contrary, a lamellar structure is exhibited in the presence of TEAB additives [Figure 5G]. The results suggest that the TEAB additive can effectively mitigate the degradation of the Zn anode surface upon cycling, avoid the drastic change of the Zn anode shape, and, therefore, improve the cycling stability. Meanwhile, as seen in the XRD patterns in Supplementary Figure 17, the peaks corresponding to $Zn_4(OH)_6SO_4 \cdot xH_2O$ by-products in the presence of TEAB additives are much weaker than those in pure ZSO electrolyte, confirming the effective mitigation of the by-product generation with the TEAB additives. We have performed a comparative analysis of the performance of Zn||Zn symmetric cells and Zn||MnO_2 full cells with existing literature to highlight the potential implications of our current work. The results are presented in Supplementary Tables 1 and 2.

CONCLUSIONS

In summary, we propose using TEAB as a non-toxic and cost-effective electrolyte additive to improve the ZMB durability during cycling. By disrupting the H-bond network in the ZSO electrolyte, TEAB effectively reduces H_2O molecule activity and inhibits side reactions such as HER and corrosion in the electrode/electrolyte interface. This results in the Zn||Zn symmetric battery demonstrating outstanding rate capability and maintaining remarkable cycle stability for 4,950 h at 1 mA cm^{-2} and 1 mAh cm^{-2}. Additionally, the Zn||Cu battery achieves an impressive average CE of up to 99.5% after 1,000 cycles. Furthermore, the Zn||MnO_2 full cell with the TEAB additives retains 91.22% of its capacity after 2,000 cycles at 3 A g^{-1}.

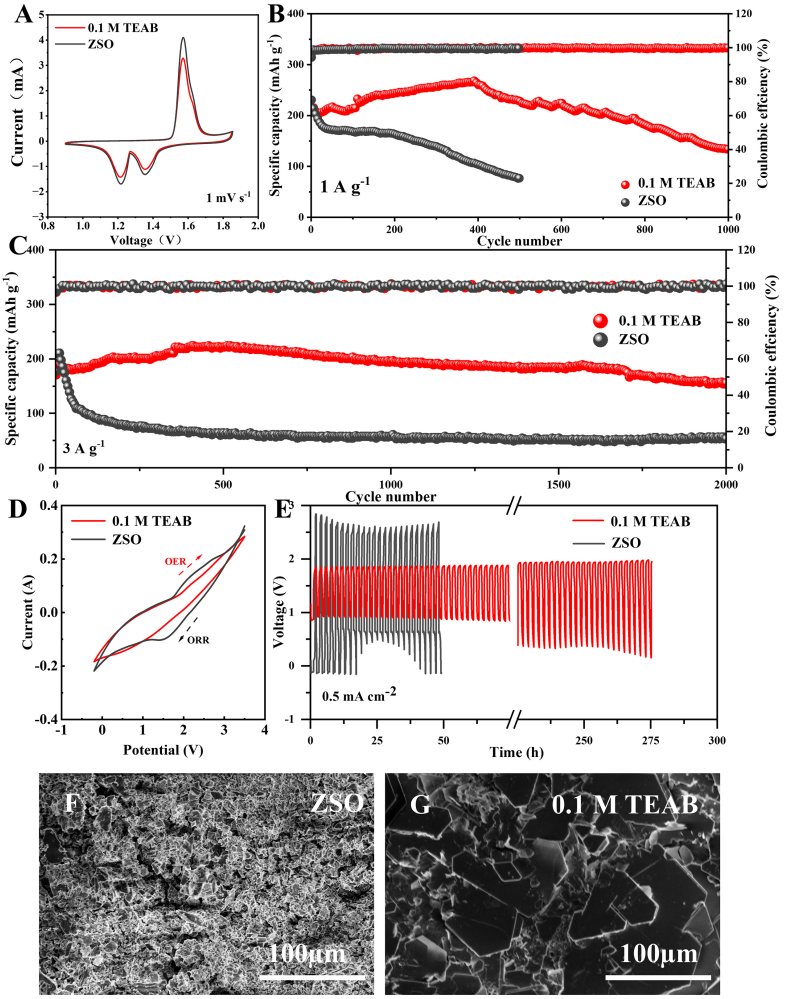

Figure 5. Electrochemical performance of Zn||MnO_2 full cells and Zn||air cells in ZSO electrolytes with and without 0.1 M TEAB additive: (A) CV curves at 1 mV s^{-1}.Cycling performance of Zn||MnO_2 cells at (B) 1 A g^{-1} and (C) 3 A g^{-1}.(D) CV curves in Zn||air cells at 10 mV s^{-1}. (E) Cycling performance of Zn||air cells. SEM images of anodes after cycling in (F) ZSO electrolyte and (G) ZSO electrolyte with 0.1 M TEAB additive.

Notably, the TEAB additive endows the Zn||air battery with a stable cycle life of up to 270 h with a reversible capacity of 616 mAh g^{-1}. This work provides an efficient electrolyte additive to successfully achieve dendrite-free Zn anodes and enhance the ZMB performance.

DECLARATIONS

Acknowledgments

We would like to thank the Analysis and Test Center, Guangdong University of Technology, for the microscopy and microanalysis of our specimens.

Authors' contributions

Methodology, investigation, measurement execution, and manuscript writing: Fang T
Investigation reviewing, measurement execution, and data analysis: Wu M
Investigation, methodology, and data analysis: Lu F

Investigation and methodology: Zhou Z
Project administration, supervision, funding acquisition, and editing: Fu Y
Resources, funding acquisition, and supervision: Shi Z

Availability of data and materials

The data supporting our work can be found in the Supplementary Materials.

Financial support and sponsorship

This work was financially supported by the National Natural Science Foundation of China (Grant No. 21905057).

Conflicts of interest

All authors declared that there are no conflicts of interest.

Ethical approval and consent to participate

Not applicable.

Consent for publication

Not applicable.

REFERENCES

1. Blanc LE, Kundu D, Nazar LF. Scientific challenges for the implementation of Zn-ion batteries. *Joule* 2020;4:771-99. DOI
2. Yang J, Yin B, Sun Y, et al. Zinc anode for mild aqueous zinc-ion batteries: challenges, strategies, and perspectives. *Nanomicro Lett* 2022;14:42. DOI PubMed PMC
3. Wang Y, Wang Z, Yang F, et al. Electrolyte engineering enables high performance zinc-ion batteries. *Small* 2022;18:e2107033. DOI
4. Xu M, Chen J, Zhang Y, Raza B, Lai C, Wang J. Electrolyte design strategies towards long-term Zn metal anode for rechargeable batteries. *J Energy Chem* 2022;73:575-87. DOI
5. Li Y, Wang Z, Cai Y, et al. Designing advanced aqueous zinc-ion batteries: principles, strategies, and perspectives. *Energy Environ Mater* 2022;5:823-51. DOI
6. Zheng Y, Yao Y, Ou J, et al. A review of composite solid-state electrolytes for lithium batteries: fundamentals, key materials and advanced structures. *Chem Soc Rev* 2020;49:8790-839. DOI
7. Schon TB, McAllister BT, Li PF, Seferos DS. The rise of organic electrode materials for energy storage. *Chem Soc Rev* 2016;45:6345-404. DOI
8. Chen Y, Kang Y, Zhao Y, et al. A review of lithium-ion battery safety concerns: the issues, strategies, and testing standards. *J Energy Chem* 2021;59:83-99. DOI
9. Liu B, Jia Y, Yuan C, et al. Safety issues and mechanisms of lithium-ion battery cell upon mechanical abusive loading: a review. *Energy Stor Mater* 2020;24:85-112. DOI
10. Chao D, Zhou W, Xie F, et al. Roadmap for advanced aqueous batteries: from design of materials to applications. *Sci Adv* 2020;6:eaba4098. DOI PubMed PMC
11. Fang G, Zhou J, Pan A, Liang S. Recent advances in aqueous zinc-ion batteries. *ACS Energy Lett* 2018;3:2480-501. DOI
12. Huang S, Zhu J, Tian J, Niu Z. Recent progress in the electrolytes of aqueous zinc-ion batteries. *Chemistry* 2019;25:14480-94. DOI PubMed
13. Park JH, Park SH, Joung D, Kim C. Sustainable biopolymeric hydrogel interphase for dendrite-free aqueous zinc-ion batteries. *Chem Eng J* 2022;433:133532. DOI
14. Ma L, Chen S, Li N, et al. Hydrogen-free and dendrite-free all-solid-state zn-ion batteries. *Adv Mater* 2020;32:e1908121. DOI
15. Li B, Zhang X, Wang T, et al. Interfacial engineering strategy for high-performance Zn metal anodes. *Nanomicro Lett* 2021;14:6. DOI PubMed PMC
16. Xie C, Li Y, Wang Q, Sun D, Tang Y, Wang H. Issues and solutions toward zinc anode in aqueous zinc-ion batteries: a mini review. *Carbon Energy* 2020;2:540-60. DOI
17. Hao J, Long J, Li B, et al. Toward high-performance hybrid Zn-based batteries via deeply understanding their mechanism and using electrolyte additive. *Adv Funct Mater* 2019;29:1903605. DOI

18. Ming J, Cao Z, Wu Y, et al. New insight on the role of electrolyte additives in rechargeable lithium ion batteries. *ACS Energy Lett* 2019;4:2613-22. DOI
19. Fang T, Liu Q, Hu A, Meng J, Fu Y, Shi Z. Dendrite-free and stable zinc-ion batteries enabled by a cation-anion synergistic regulation additive. *J Power Sources* 2023;581:233521. DOI
20. Bayaguud A, Luo X, Fu Y, Zhu C. Cationic surfactant-type electrolyte additive enables three-dimensional dendrite-free zinc anode for stable zinc-ion batteries. *ACS Energy Lett* 2020;5:3012-20. DOI
21. Sun T, Zheng S, Du H, Tao Z. Synergistic effect of cation and anion for low-temperature aqueous zinc-ion battery. *Nanomicro Lett* 2021;13:204. DOI PubMed PMC
22. Chen P, Zhang K, Tang D, et al. Recent progress in electrolytes for Zn-air batteries. *Front Chem* 2020;8:372. DOI PubMed PMC
23. Lin MH, Huang CJ, Cheng PH, Cheng JH, Wang CC. Revealing the effect of polyethylenimine on zinc metal anodes in alkaline electrolyte solution for zinc-air batteries: mechanism studies of dendrite suppression and corrosion inhibition. *J Mater Chem A* 2020;8:20637-49. DOI
24. Chen CY, Matsumoto K, Kubota K, Hagiwara R, Xu Q. A room-temperature molten hydrate electrolyte for rechargeable zinc-air batteries. *Adv Energy Mater* 2019;9:1900196. DOI
25. Kapaev RR, Ohayon A, Sonoo M, Tzadikov J, Shalom M, Noked M. Structure-performance relations for carbons in Zn-air battery cathodes with non-alkaline electrolytes. *Electrochim Acta* 2023;456:142462. DOI
26. Wu WF, Yan X, Zhan Y. Recent progress of electrolytes and electrocatalysts in neutral aqueous zinc-air batteries. *Chem Eng J* 2023;451:138608. DOI
27. Wang C, Li J, Zhou Z, et al. Rechargeable zinc-air batteries with neutral electrolytes: recent advances, challenges, and prospects. *EnergyChem* 2021;3:100055. DOI
28. Wang K, Pei P, Wang Y, Liao C, Wang W, Huang S. Advanced rechargeable zinc-air battery with parameter optimization. *Appl Energy* 2018;225:848-56. DOI
29. Sun W, Küpers V, Wang F, Bieker P, Winter M. A non-alkaline electrolyte for electrically rechargeable zinc-air batteries with long-term operation stability in ambient air. *Angew Chem Int Ed* 2022;61:e202207353. DOI
30. Liu Z, Wang R, Gao Y, et al. Low-cost multi-function electrolyte additive enabling highly stable interfacial chemical environment for highly reversible aqueous zinc ion batteries. *Adv Funct Mater* 2023;33:2308463. DOI
31. Ghavami RK, Rafiei Z, Tabatabaei SM. Effects of cationic CTAB and anionic SDBS surfactants on the performance of Zn-MnO_2 alkaline batteries. *J Power Sources* 2007;164:934-46. DOI
32. Chang C, Hu S, Li T, et al. A robust gradient solid electrolyte interphase enables fast Zn dissolution and deposition dynamics. *Energy Environ Sci* 2024;17:680-94. DOI
33. Wan S, Song K, Chen J, et al. Reductive competition effect-derived solid electrolyte interphase with evenly scattered inorganics enabling ultrahigh rate and long-life span sodium metal batteries. *J Am Chem Soc* 2023;145:21661-71. DOI
34. Gou Q, Luo H, Zhang Q, et al. Electrolyte regulation of bio-inspired zincophilic additive toward high-performance dendrite-free aqueous zinc-ion batteries. *Small* 2023;19:e2207502. DOI
35. Zhi L, Li T, Liu X, Yuan Z, Li X. Functional complexed zincate ions enable dendrite-free long cycle alkaline zinc-based flow batteries. *Nano Energy* 2022;102:107697. DOI
36. Zhou W, Chen M, Tian Q, Chen J, Xu X, Wong C. Cotton-derived cellulose film as a dendrite-inhibiting separator to stabilize the zinc metal anode of aqueous zinc ion batteries. *Energy Stor Mater* 2022;44:57-65. DOI
37. Zhang D, Cao J, Chanajaree R, et al. Reconstructing the anode interface and solvation shell for reversible zinc anodes. *ACS Appl Mater Interfaces* 2023;15:11940-8. DOI
38. Sumboja A, Ge X, Zheng G, et al. Durable rechargeable zinc-air batteries with neutral electrolyte and manganese oxide catalyst. *J Power Sources* 2016;332:330-6. DOI